Carrier transport in reverse-biased graphene/semiconductor Schottky junctions

D. Tomer,[1,a)] S. Rajput,[1] L. J. Hudy,[1] C. H. Li,[2] and L. Li[1]
[1]*Department of Physics, University of Wisconsin, Milwaukee, Wisconsin 53211, USA*
[2]*Naval Research Laboratory, Washington, DC 20375, USA*

(Received 9 February 2015; accepted 17 April 2015; published online 1 May 2015)

Reverse-biased graphene (Gr)/semiconductor Schottky diodes exhibit much enhanced sensitivity for gas sensing. However, carrier transport across these junctions is not fully understood yet. Here, Gr/SiC, Gr/GaAs, and Gr/Si Schottky junctions under reverse bias are investigated by temperature-dependent current-voltage measurements. A reduction in barrier height with increasing bias is observed for all junctions, suggesting electric-field enhanced thermionic emission. Further analysis of the field dependence of the reverse current reveals that while carrier transport in Gr/SiC Schottky junctions follows the Poole-Frenkel mechanism, it deviates from both the Poole-Frankel and Schottky mechanisms in Gr/Si and Gr/GaAs junctions, particularly for low temperatures and fields. © *2015 AIP Publishing LLC*. [http://dx.doi.org/10.1063/1.4919727]

The high electrical conductivity, tunable Fermi level, and two-dimensional nature of graphene (Gr) make it a promising material for electronic, optoelectronic, and sensing applications.[1–3] In particular, when graphene is interfaced with semiconductors it forms Schottky junctions,[4] which can be used in solar cells,[5,6] photo-detectors,[7,8] three-terminal transistors,[9] and gas sensors.[10–12] Carrier transport across these Schottky junctions generally follows the thermionic emission (TE) theory.[4,13–18] The characteristic junction parameters, such as the ideality factor (η) and Schottky barrier height (SBH), however, often exhibit non-ideal behavior (e.g., $\eta \sim 1.5$–30) and strong temperature dependence.[16–18] This can be attributed to intrinsic and extrinsic spatial inhomogeneities, including graphene ripples, ridges, substrate steps, and additional interface states typically found in graphene heterojunctions.[19–21] In recent work, a modified TE model assuming a Gaussian distribution of the barrier height offers a better account of carrier transport in these graphene/semiconductor Schottky junctions.[22,23] Moreover, Landauer transport mechanism is also suggested to describe the properties of nearly ideal ($\eta \sim 1.08$) Gr/Si Schottky junctions.[24]

Under reverse bias, these graphene Schottky junctions additionally exhibit much improved performance for gas sensing compared to field effect devices, primarily due to the exponential dependence of the reverse current on the SBH.[12,25–27] However, much less is known about carrier transport across these junctions under reverse bias. Recent work has shown strong bias dependent SBHs and non-saturating reverse bias current in Gr/n-Si junctions, which is attributed to interfacial charges.[24] Here, we present systematic studies of the temperature- and electric-field dependence of graphene Schottky junction current under reverse bias. We find that while carrier transport in reverse-biased Gr/SiC Schottky junction follows the Poole-Frenkel mechanism, it deviates from both the Poole-Frankel and the Schottky emission mechanisms in Gr/Si and Gr/GaAs junctions, particularly for low temperatures and electric fields.

The Schottky junctions are fabricated by transferring chemical vapor deposited (CVD) monolayer graphene onto hydrogen-terminated hexagonal SiC (both the (0001) Si-face and $(000\bar{1})$ C-face), Si (111), and sulfur-terminated GaAs (100) substrates. The H-termination of the SiC substrates is obtained by annealing the as-received SiC wafers at 1600 °C in H_2/Ar atmosphere for 15 min.[19,28] This process removes polishing scratches from the SiC wafers, and produces atomically flat step-terrace morphology with a chemically inert surface terminated with hydrogen.[19] Si and GaAs substrates are first cleaned by RCA solutions, followed by dipping into 49% HF + 40% NH_4F (1:7) and NH_4S (40%) solutions to terminate with hydrogen[29] and sulfur,[30] respectively. For all diodes, the top electrode is formed by 150/10 nm Au/Cr deposited by e-beam evaporation (pressure $\sim 2 \times 10^{-6}$ Torr) at room temperature, insulated by 100 nm SiO_2. Metal back contact to SiC is achieved by sputter depositing 100 nm Ni and annealing at 600 °C in Ar environment.[22] On GaAs, multilayer Au/Ni/AuGe (100/20/50 nm) is similarly deposited by e-beam evaporation at room temperature, followed by annealing at ~400 °C in forming gas. For Si, Ohmic back contact is made by conducting silver paste. Monolayer CVD graphene (Graphene Platform, Inc.) is transferred onto the patterned top contacts in the final step using standard PMMA-based method.[31] Temperature dependent I-V measurements are carried out between 250 and 340 K.

All junctions exhibit rectifying behaviors, as shown, for example, in Fig. 1(a) for Gr/GaAs at 310 K.[22,23] Under the reverse bias, however, the current rises with increasing bias voltage, as better seen in the semi-logarithmic plots for Gr/Si-SiC and GaAs diodes between 250 and 340 K (Figs. 1(b) and 1(c)). This is clearly inconsistent with the simple thermionic emission picture,[32] where for $V < -3\,k_BT/q$ (k_B is the Plank constant and q is the charge), the reserve bias current should saturate

$$I(T) = AA^*T^2 \exp\left(\frac{-q\phi_{b0}}{k_BT}\right), \quad (1)$$

where A is the junction contact area (~1.96 mm^2 for Gr/SiC and 1.62 mm^2 for Gr/Si and Gr/GaAs), A^* is the effective

[a)]Author to whom correspondence should be addressed. Electronic mail: dtomer@uwm.edu

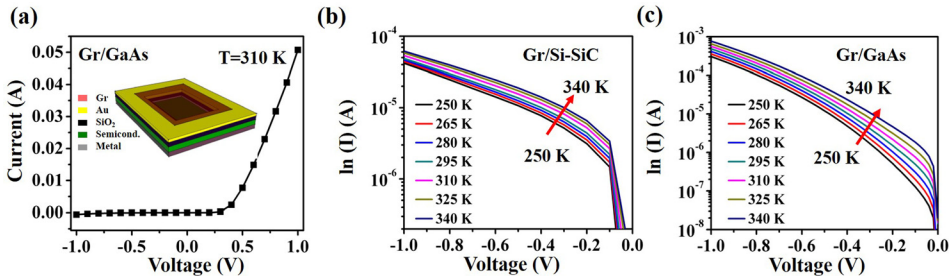

FIG. 1. (a) I-V curve of Gr/GaAs Schottky junction at 310 K showing a rectifying behavior (inset: schematic diagram of the devices). Temperature dependent I-V characteristics of (b) Gr/Si-SiC and (c) Gr/GaAs Schottky junctions in the reverse bias regime between 250 and 340 K.

Richardson constant (1.46×10^6, 1.12×10^6, and 0.41×10^4 $Am^{-2}K^{-2}$ for SiC, Si, and GaAs, respectively), and ϕ_{b0} is the zero bias barrier height. Similar behaviors are also observed for Gr/C-SiC and Gr/Si Schottky junctions.

The non-saturating current under reverse bias suggests that the barrier height is a function of the bias voltage, as calculated following Eq. (1) and shown in Fig. 2. At 310 K, the calculated ϕ_{b0} decreases with increasing reverse bias for all junctions, similar to previous work on Gr/Si Schottky junctions,[24] with the Gr/GaAs junction showing a lower barrier and larger variation. These behaviors suggest low interfacial states at these graphene Schottky junctions, since they are known to pin the Fermi level in the semiconductor, which leads to reverse current saturation in conventional metal/semiconductor junctions.[33]

To account for the reduction of barrier height with increasing reverse bias, electric-field enhanced thermionic emission is further investigated following the Poole-Frenkel[34] and Schottky[35] emission mechanisms. The reverse current considering Poole-Frenkel emission is given by[34]

$$I \propto E \exp\left(\frac{q}{k_B T}\sqrt{\frac{qE}{\pi\varepsilon_s}}\right), \tag{2}$$

Whereas in the case of Schottky emission, it is given by[34]

$$I \propto T^2 \exp\left(\frac{q}{2k_B T}\sqrt{\frac{qE}{\pi\varepsilon_s}}\right). \tag{3}$$

Here, E is the applied electric field, calculated by $E = \sqrt{\frac{2qN_D}{\varepsilon_s}\left(V + V_{bi} - \frac{k_B T}{q}\right)}$, where ε_s is the relative dielectric constant of the semiconductor (~9.66 for SiC[36]), N_D is the donor density of the semiconductor (~10^{18} cm^{-3}),[22] V is the applied bias, and V_{bi} is the built-in potential. The built-in potential is a function of forward-biased SBH and the effective density of states in semiconductor conduction band (N_C) at room temperature,[32] taken as 1.69×10^{19} for Si-SiC.[36] The mean SBH values of 1.16 eV are taken for Gr/Si-SiC Schottky junction.[22]

Thus, if the Poole-Frenkel effect contributes to the reverse current, then the plot of *ln (I/E)* versus $E^{1/2}$ should be linear. Similarly, if a linear plot is found for *ln* (I/T^2) versus $E^{1/2}$, then the Schottky mechanism is present. Figures 3(a) and 3(b) show plots of *ln (I/E)* and *ln* (I/T^2) as a function of $E^{1/2}$, respectively, for the Gr/Si-SiC Schottky junction. Clearly, both are near linear for all temperatures, indicating that both Schottky and Poole-Frenkel emissions are present.

To distinguish which mechanism the carrier transport is dominated by, we calculate the emission coefficient as follows:[34]

$$S = \frac{q}{nkT}\sqrt{\frac{q}{\pi\varepsilon_s}}, \tag{4}$$

where $n = 1$ for Poole-Frenkel emission and $n = 2$ for Schottky emission. The calculated coefficients are compared with that obtained by curve fitting for both Poole-Frenkel and Schottky emissions at different temperatures, as shown in Table I between 250 and 340 K for the Gr/Si-SiC Schottky junction. For the Poole-Frenkel emission, the experimental values are almost ~2–2.3 times that of the calculated value at all temperatures. For Schottky emission, the experimental values are ~3.5 times larger. Similar trend is also found for Gr/C-SiC junction. Thus, carrier transport in graphene/SiC Schottky junctions under reverse bias is more consistent with the Poole-Frenkel mechanism for these temperatures.

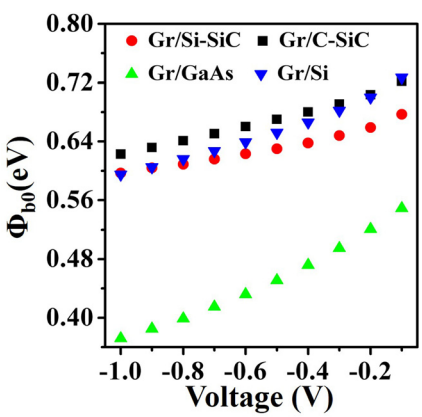

FIG. 2. Calculated Schottky barrier height ϕ_{b0} as a function of reverse bias voltage at 310 K.

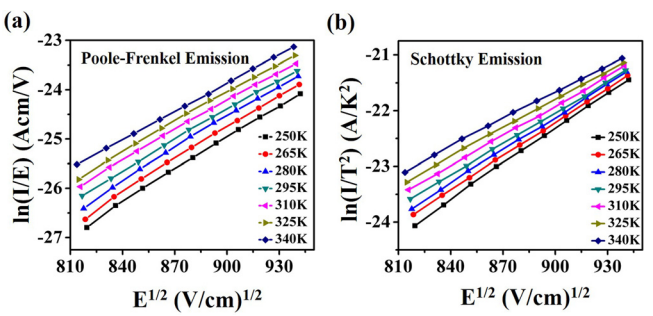

FIG. 3. Temperature dependent (a) Poole-Frenkel and (b) Schottky emission plots for Gr/Si-SiC Schottky junctions.

TABLE I. Comparison of calculated and experimental Poole-Frenkel and Schottky emission coefficients between 250 and 340 K for the Gr/Si-SiC Schottky junction.

	Poole-Frenkel emission $(V/cm)^{1/2}$		Schottky emission $(V/cm)^{1/2}$	
Temperature (K)	Calculated	From fit	Calculated	From Fit
250	0.0113	0.0224	0.0056	0.0213
265	0.0107	0.0219	0.0053	0.0202
280	0 0101	0.0215	0.0050	0 0198
295	0.0096	0.0206	0.0048	0.0185
310	0.0091	0.0199	0.0046	0.0178
325	0.0087	0.0194	0.0044	0.0171
340	0.0083	0.0191	0.0041	0.0161

Similar analysis was performed for Gr/GaAs and Gr/Si junctions, as shown in Fig. 4, where ε_s is taken as 12.9 (Ref. 37) and 11.7;[38] $N_D \sim 10^{16}$ and $10^{17}\,cm^{-3}$, $N_C = 4.70 \times 10^{17}$ and $2.86 \times 10^{19}\ cm^{-3}$ for GaAs and Si, respectively,[36] and the mean SBH values of 1.14 and 0.76 eV are taken for Gr/Si and Gr/GaAs Schottky junctions.[23] For Gr/GaAs (Figs. 4(a) and 4(b)), both the Poole-Frenkel and the Schottky emission plots are linear above 310 K, suggesting a possible co-existence of both mechanisms at higher temperatures. Again the Poole-Frenkel and Schottky emission coefficients must be considered to identify their contributions to carrier transport. At 340 K, the Poole-Frenkel coefficient obtained from the fit is 0.119 $(V/cm)^{1/2}$, ~16 times the calculated value of 0.007 $(V/cm)^{1/2}$. On the other hand, for the Schottky emission, the experimental value (0.128 $(V/cm)^{1/2}$) is ~35 times greater than that calculated (0.0036 $(V/cm)^{1/2}$).

For the Gr/Si Schottky junction, the Poole-Frenkel and Schottky emission plots are shown in Figs. 4(c) and 4(d). In both cases, although they are still linear at 340 K, non-linearity is found for temperatures below 310 K, particularly in the low electric field region. Fittings to the linear plots at 340 K yield an experimental emission coefficient of 0.0615 $(V/cm)^{1/2}$, ~8 times greater than the calculated value (0.0076 $(V/cm)^{1/2}$) for the Poole-Frenkel mechanism. For the Schottky emission, the experimental value (0.0658 $(V/cm)^{1/2}$) is ~17 times greater than that calculated (0.0038 $(V/cm)^{1/2}$).

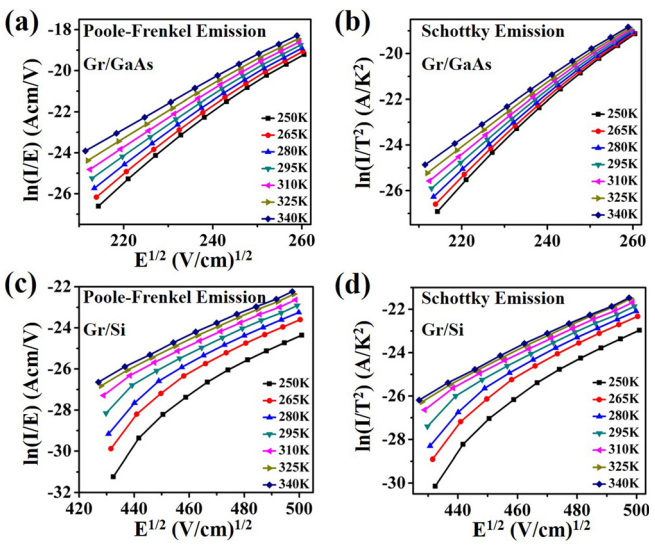

FIG. 4. Temperature dependent ((a) and (c)) Poole-Frenkel and ((b) and (d)) Schottky emission plots for Gr/GaAs and Gr/Si Schottky junctions.

These results suggest that carrier transport in the reverse-biased Gr/GaAs and Gr/Si Schottky diodes deviate from the Poole-Frenkel and Schottky emission, particularly at low temperatures and electric fields. This may be due to the much larger depletion width, ~0.1–0.5 μm, for the Gr/Si and Gr/GaAs Schottky junctions, comparable to that reported for Gr/Si.[16] For comparison, the depletion width is only ~35–48 nm for the Gr/Si-SiC junctions. In addition, other conduction mechanisms such as bias dependent doping,[24] i.e., electric field dependence of the Fermi level in graphene, should also be taken into account in these non-linear regimes.

In conclusion, reverse-biased Gr/SiC, Gr/GaAs, and Gr/Si Schottky junctions are studied by temperature dependent I-V measurements between 250 and 340 K. A reduction in barrier height with increasing reverse bias is observed for all junctions, consistent with electric-field enhanced thermionic emission. Analysis of the field dependence of the reverse current reveals that while carrier transport in Gr/SiC Schottky junctions follows the Poole-Frenkel mechanism, it deviates from both the Poole-Frankel and the Schottky mechanisms in Gr/Si and Gr/GaAs junctions, particularly in the low temperature and field regimes, where field dependent doping in graphene should also be taken into account. Our findings present the direct experimental evidence for electric-field enhanced thermionic emission in graphene/semiconductor Schottky junctions under reverse bias, providing insights into carrier transport mechanisms that can help improve functionalities of graphene-based devices.

Research supported by the U.S. Department of Energy, Office of Basic Energy Sciences, Division of Materials Sciences and Engineering under Award No. DE-FG02-07ER46228.

[1]K. S. Novoselov, A. K. Geim, S. V. Morozov, D. Jiang, Y. Zhang, S. V. Dubonos, I. V. Grigorieva, and A. A. Firsov, Science **306**, 666 (2004).
[2]Y. J. Yu, Y. Zhao, S. Ryu, L. E. Brus, K. S. Kim, and P. Kim, Nano Lett. **9**, 3430 (2009).
[3]G. Chen, T. M. Paronyan, and A. Harutyunyan, Appl. Phys. Lett. **101**, 053119 (2012).
[4]S. Tongay, M. Lemaitre, X. Miao, B. Gila, B. R. Appleton, and A. F. Hebard, Phys. Rev. X **2**, 011002 (2012).
[5]L. Lancellotti, T. Polichetti, F. Ricciardella, O. Tari, S. Gnanapragasam, S. Daliento, and G. Di. Francia, Thin Solid Films **522**, 390 (2012).
[6]W. Jie, F. Zheng, and J. Hao, Appl. Phys. Lett. **103**, 233111 (2013).

[7]Y. An, A. Behnam, E. Pop, and A. Ural, Appl. Phys. Lett. **102**, 013110 (2013).
[8]L. Luo, J. Chen, M. Z. Wang, H. Hu, C. Y. Wu, Q. Li, L. Wang, J. A. Huang, and F. X. Liang, Adv. Funct. Mater. **24**, 2794 (2014).
[9]H. Yang, J. Heo, S. Park, H. J. Song, D. H. Seo, K. E. Byun, P. Kim, I. Yoo, H. J. Chung, and K. Kim, Science **336**, 1140 (2012).
[10]S. Rumyantsev, G. Liu, M. S. Shur, and R. A. Potyrailo, Nano Lett. **12**, 2294 (2012).
[11]Y. Du, Q. Xue, Z. Zhang, and F. Xia, Mater. Lett. **135**, 151 (2014).
[12]A. Singh, Md. A. Uddin, T. Sudarshan, and G. Koley, Small **10**, 1555 (2014).
[13]M. Amirmazlaghani, F. Raissi, O. Habibpour, J. Vukusic, and J. Stake, IEEE J. Quantum Electron. **49**, 589 (2013).
[14]M. Mohammed, Z. Li, J. Cui, and T. P. Chen, Nanoscale Res. Lett. **7**, 302 (2012).
[15]G. Kalita, R. Hirano, M. E. Ayhan, and M. Tanemura, J. Phys. D: Appl. Phys. **46**, 455103 (2013).
[16]X. Li, H. Zhu, K. Wang, A. Cao, J. Wei, C. Li, Y. Jia, Z. Li, X. Li, and D. Wu, Adv. Mater. **22**, 2743 (2010).
[17]C. C. Chen, M. Aykol, C. C. Chang, A. F. J. Levi, and S. B. Cronin, Nano Lett. **11**, 1863 (2011).
[18]T. Hosseini, D. Tomer, S. Rajput, L. Li, and N. Kouklin, Appl. Phys. Lett. **105**, 223107 (2014).
[19]S. Rajput, M. Chen, Y. Liu, Y. Y. Li, M. Weinert, and L. Li, Nat. Commun. **4**, 2752 (2013).
[20]S. Shivaraman, L. H. Herman, F. Rana, J. Park, and M. G. Spencer, Appl. Phys. Lett. **100**, 183112 (2012).
[21]M. J. Tadjer, T. J. Anderson, R. L. Myers-Ward, V. D. Wheeler, L. O. Nyakiti, Z. Robinson, C. R. Eddy, D. K. Gaskill, A. D. Koehler, K. D. Hobart, and F. J. Kub, Appl. Phys. Lett. **104**, 073508 (2014).
[22]D. Tomer, S. Rajput, L. J. Hudy, C. H. Li, and L. Li, Appl. Phys. Lett. **105**, 021607 (2014).
[23]D. Tomer, S. Rajput, L. J. Hudy, C. H. Li, and L. Li, e-print arXiv:1503.03766.
[24]D. Sinha and J. U. Lee, Nano Lett. **14**, 4660 (2014).
[25]R. Pearce, T. Iakimov, M. Andersson, L. Hultman, A. L. Spetz, and R. Yakimova, Sens. Actuators, B **155**, 451 (2011).
[26]N. Hu, Z. Yang, Y. Wang, L. Zhang, Y. Wang, X. Huang, H. Wei, L. Wei, and Y. Zhang, Nanotechnology **25**, 025502 (2014).
[27]H. Y. Kim, K. Lee, N. Mcevoy, C. Yim, and G. S. Duesberg, Nano Lett. **13**, 2182 (2013).
[28]S. Dogan, D. Johnstone, F. Yun, S. Sabuktagin, J. Leach, A. A. Baski, H. Morkoc, and B. Ganguly, Appl. Phys. Lett. **85**, 1547 (2004).
[29]J. I. Dalap, B. Doris, Q. Deng, M. C. Downer, J. K. Lowell, and A. C. Diebold, Appl. Phys. Lett. **64**, 2139 (1994).
[30]H. H. Lee, R. J. Racicot, and S. H. Lee, Appl. Phys. Lett. **54**, 724 (1989).
[31]J. W. Suk, A. Kitt, C. W. Magnuson, Y. Sao, S. Ahmed, J. An, A. K. Swan, B. B. Goldberg, and R. S. Ruoff, ACS Nano **5**, 6916 (2011).
[32]S. M. Sze, *Physics of Semiconductor Devices*, 2nd ed. (Wiley, New York, 1981).
[33]Y. Zhou, W. Han, Y. Wang, F. Xiu, J. Zou, R. K. Kawakami, and K. L. Wang, Appl. Phys. Lett. **96**, 102103 (2010).
[34]V. Janardhanam, A. Jyothi, K. S. Ahn, and C. J. Choi, Thin Solid Films **546**, 63 (2013).
[35]J. Lin, S. Banerjee, J. Lee, and C. Teng, IEEE Electron Device Lett. **11**, 191 (1990).
[36]J. Lutz, H. Schlangenotto, U. Scheuermann, and R. D. Doncker, *Semiconductor Power Devices* (Springer, 2011).
[37]R. E. Neidert, Electron. Lett. **16**(7), 244 (1980).
[38]J. C. Anderson, *Material Science for Engineers*, 5th ed. (Nelson Thornes Ltd., 2009).